Chapter 2

Basic Principles of Quasicrystallography

Conventional crystals are constructed by a periodic repetition of a single unit-cell. This periodic long-range order only agrees with two-, three-, four- and sixfold point symmetries. Long-range order in crystals without periodicity seemed impossible [23]. Therefore, the discovery of a fivefold rotational symmetry in a sharp diffraction pattern from Al-Mn alloys in 1984 was very surprising [1]. In order to explain the diffraction pattern another type of long-range order had to be introduced. Eventually in 1992, the International Union of Crystallography redefined a crystal as 'a solid having an essentially discrete diffraction pattern' [2].

This chapter introduces general concepts in quasicrystallography. First, it will be explained why only certain symmetries agree with translational long-range order. In order to illustrate the existence of long-range order without periodicity, the prominent one-dimensional example of the Fibonacci sequence will be discussed first. The Penrose tiling, featuring quasiperiodicity in two dimensions, will subsequently be introduced. Both can be derived from a periodic lattice in higher dimensional space as will be discussed. Then other important principles in quasicrystallography such as phasons and approximants will be introduced before presenting structural properties of the Al-Ni-Co and Al-Pd-Mn quasicrystals used in the experimental work in this thesis.

2.1 Forbidden Symmetries in Periodic Systems

The aim of this section is to show that certain point symmetries cannot be related to periodic long-range order. For simplicity, only two-dimensional planes will be considered. It is readily visualized that a two-dimensional plane can be tiled by regular rectangles, triangles, squares or

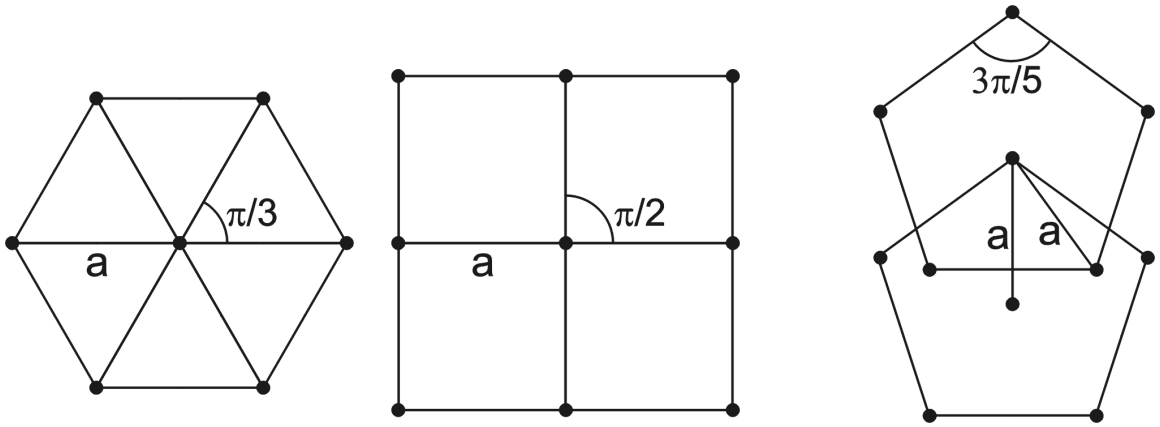

Figure 2.1: Allowed and forbidden symmetries in periodic systems: A plane can be tiled by triangles and squares, while pentagons leave gaps. The disagreement of a pentagonal tiling with periodicity is indicated by pentagon shifted by the lattice parameter a.

hexagons. This can be explained by the fact that 2π is a multiple of these polygons' vertex angles. Each lattice point can be surrounded by four rectangles since $4 \times \pi/2 = 2\pi$, by six triangles since $6 \times \pi/3 = 2\pi$, by four squares since $4 \times \pi/2 = 2\pi$, and likewise by three hexagons since $3 \times 2\pi/3 = 2\pi$. Consequently, starting from one lattice point and applying a translation along the polygons' edges yields a lattice point of the same local arrangement and periodicity is achieved.

In contrast, translating a lattice point of local fivefold symmetry along the lattice parameter a as indicated in figure 2.1 leads to a lattice point which cannot exhibit the same fivefold symmetry. Assuming that it would have a fivefold symmetry would require distances between atoms which are smaller than a, therefore contradicting the assumption of periodicity with lattice parameter a.

An equivalent argument can be given for any other polygon not satisfying the condition of 2π being a multiple of the vertex angles [24]. Suitable candidates for polygons related to periodicity are only the ones mentioned above. This can be inferred from the vertex angles $(n-2)\pi/n$, with n the number of edges.

2.2 The Fibonacci Sequence

The Fibonacci sequence is a prominent example for a one-dimensional quasiperiodic structure. There are several methods to obtain the Fibonacci sequence, which consists of two types of segments, L (long) and S (short). One recipe is to start with a segment and follow the substitution

rule S → L and L → LS to obtain successive strings of increasing length.

generation	section F	Fibonacci number
1	L	1
2	LS	2
3	LSL	3
4	LSLLS	5
5	LSLLSLSL	8
6	LSLLSLSLLSLLS	13

For the Fibonacci sequence, the segment ratio L/S is equal to the golden mean $\tau = 2\cos 36^\circ = (1+\sqrt{5})/2 = 1.618034....$ The limit of the frequency ratio of L and S is also the golden mean τ. This interesting irrational number is often encountered when considering fivefold symmetries, as e.g. in a pentagon the ratio of the distances (center to vertex) : (center to mid-edge) equals $\tau/2$.

One other important property of the Fibonacci chain is its self-similarity, meaning that by an inflation or deflation, i.e., by a substitution rule of the kind $L \rightarrow F_{n+1}$ and $S \rightarrow F_n$, where n denotes the generation number, another Fibonacci sequence of different length arises.

2.2.1 Quasiperiodicity Generated from Higher Dimensional Space

Another method to construct a Fibonacci sequence, and a very important concept in quasicrystallography, is the embedding in higher dimensional space. By the cut- or projection-method, a quasiperiodic structure of N dimensions can be created from a periodic structure in n > N dimensional space [24-28]. The cut method is illustrated by the example of the 1-dimensional Fibonacci sequence in the left column of figure 2.2.

The starting point is a regular square lattice of lattice parameter a, where the lattice vectors $\vec{a_1}$, $\vec{a_2}$ are rotated by an angle α with respect to the cartesian coordinate axes x and y, respectively. The lattice can then be expressed as

$$\rho(\vec{r}) = \sum_{n_1,n_2} \delta(\vec{r} - n_1\vec{a_1} - n_2\vec{a_2}) \ . \tag{2.1}$$

The hypercrystal is now described by decorating the lattice with hyperatoms (atomic surfaces). Decorating the lattice with hyperatoms (HA), in this case a simple one-dimensional line, corresponds to a convolution

$$\rho' = \rho * HA \tag{2.2}$$

with

$$HA(x,y) = \delta(x)f(y), \text{where} f(y) = \begin{cases} 1, & \text{if } -\Delta/2 \le y \le \Delta/2 \\ 0, & \text{if } y < -\Delta/2 \text{ and } y > \Delta/2 \end{cases} \tag{2.3}$$

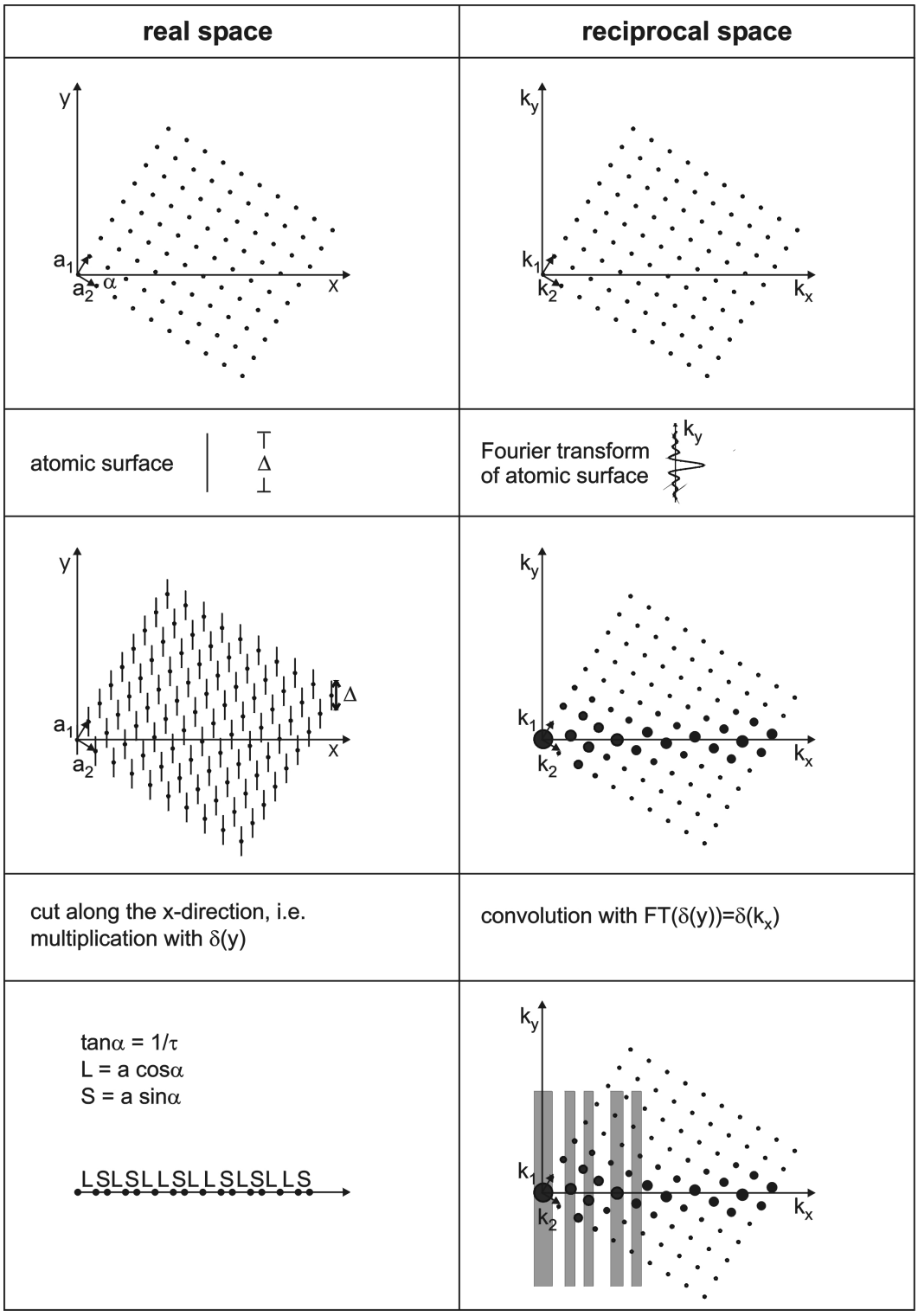

Figure 2.2: Illustration of the higher dimensional concept: The left column describes the cut method to derive a Fibonacci sequence from a periodic square lattice in two dimensions. An equivalent treatment of the lattice in reciprocal space (right column) explains, why an aperiodic structure has a sharp discrete and dense diffraction pattern. For clarity, only a few diffraction peaks are indicated by gray bars.

and $\Delta = a(\cos\alpha + \sin\alpha)$ the width of the atomic surface. A cut of the decorated lattice along the x-axis is mathematically a multiplication with $\delta(y)$, yielding a sequence with two segments, $L = a\cos\alpha$ and $S = a\sin\alpha$. If $\alpha = \arctan 1/\tau$, then $L/S = \tau$, and the sequence is the Fibonacci sequence defined above.

Thus, each position in the sequence can be described by two indices, say h_1h_2, which are the indices of the square lattice. Hence, although the structure is 1-dimensional, two independent indices are needed to characterize the real or reciprocal space positions.

2.2.2 The Diffraction Pattern of the Fibonacci Sequence

At first sight it might be surprising that an aperiodic structure can have a diffraction pattern. The mathematical clue to understand its appearance is the previously described approach based on a periodic structure in higher dimensional space. If the equivalent of each step in real space to construct the Fibonacci sequence is carried out in reciprocal space, it becomes evident that a quasicrystal does indeed show a discrete, dense diffraction pattern.

One basic rule to follow in the derivation of reciprocal space is the fact that the Fourier transform of a convolution is the product of the functions' Fourier transform and vice versa [29]:

$$FT(f * g) = FT(f) \times FT(g) \tag{2.4}$$

$$FT(f \times g) = FT(f) * FT(g) \tag{2.5}$$

The reciprocal of the square lattice with lattice parameter a is a square lattice with basis vectors $\vec{k_1}$ and $\vec{k_2}$, each of length $2\pi/a$ and rotated by an angle α from the reciprocal axes k_x and k_y. Hence, the lattice is described by

$$\hat{\rho}(\vec{k}) = \sum_{n_1,n_2} \delta(\vec{k} - n_1\vec{k_1} - n_2\vec{k_2}) \tag{2.6}$$

$$= \sum_i \delta(\vec{k} - \vec{G}_i) \tag{2.7}$$

where $\vec{G}_i$ denotes reciprocal lattice vectors.

The convolution with the hyperatoms in real space corresponds to a multiplication with the Fourier transform of the hyperatom

$$FT(HA) = 2\frac{\sin\frac{\Delta}{2}k_y}{k_y} \tag{2.8}$$

in reciprocal space resulting in an intensity modulation of the Bragg points

$$\hat{\rho}_{HA}(\vec{k}) = \sum_i 2\frac{\sin\frac{\Delta}{2}k_y}{k_y}\delta(\vec{k} - \vec{G}_i)\ . \tag{2.9}$$

As depicted in the center of the right column in figure 2.2, the intensity therefore decreases with the distance of the Bragg peak from the k_x-axis (the influence of the sinusoidal variation is neglected here).

The last step in real space, the multiplication by $\delta(y)$, is equivalent to the convolution with $FT(\delta(y)) = \delta(k_x)$. Thus,

$$\begin{aligned}
\hat{\rho}_{Fib}(\vec{k}) &= \int \delta(k'_x) \sum_i 2\frac{\sin\frac{\Delta}{2}(k_y - k'_y)}{k_y - k'_y}\delta(\vec{k} - \vec{k}' - \vec{G}_i)dk'_x dk'_y && (2.10)\\
&= \sum_i \int \delta(k'_x) 2\frac{\sin\frac{\Delta}{2}(k_y - k'_y)}{k_y - k'_y}\delta(k_x - k'_x - G_{ix})\delta(k_y - k'_y - G_{iy})dk'_x dk'_y && (2.11)\\
&= \sum_i \delta(k_x - G_{ix}) \int 2\frac{\sin\frac{\Delta}{2}(k_y - k'_y)}{k_y - k'_y}\delta(k_y - k'_y - G_{iy})dk'_y && (2.12)\\
&= \sum_i \delta(k_x - G_{ix}) 2\frac{\sin\frac{\Delta}{2}G_{iy}}{G_{iy}} \ . && (2.13)
\end{aligned}$$

The intensity of each diffraction spot is then given by the sum of all spots falling into the same δ-bar ('projection'). The thickness of those bars in figure 2.2 indicates the intensity associated to the diffraction spot. If, as required for the Fibonacci sequence, the angle α is chosen such that $\tan\alpha$ is irrational, the k_x-components of all spots are different and the spacing of the δ-bars in the last picture of figure 2.2 is dense and discrete. However, due to the intensity modulation of the spots a hierarchy is observed, leading to sharp strong Bragg peaks and to infinitely many weak spots in diffraction patterns of quasicrystals. Often in quasicrystallography, the coordinate axes x and y are called parallel (or physical) and perpendicular space, respectively. Thus, equation 2.13 reads

$$\hat{\rho}_{Fib}(\vec{k}) = \sum_i \delta(k_\parallel - G_{i\parallel}) 2\frac{\sin\frac{\Delta}{2}G_{i\perp}}{G_{i\perp}} \ . \qquad (2.14)$$

Generally, the larger the perpendicular space component the lower is the intensity of the corresponding Bragg peak. The reciprocal lattice vectors are generated by

$$\begin{aligned}
G_{1\parallel} &= a^* \sin\alpha = \frac{2\pi}{S}\sin^2\alpha && (2.15)\\
G_{2\parallel} &= a^* \cos\alpha = \frac{2\pi}{L}\cos^2\alpha \ . && (2.16)
\end{aligned}$$

For $\tan\alpha = \frac{1}{\tau}$ as required for the Fibonacci sequence

$$\begin{aligned}
G_{1\parallel} &= \frac{2\pi}{S}\frac{1}{\tau^2+1} && (2.17)\\
G_{2\parallel} &= \frac{2\pi}{L}\frac{\tau^2}{\tau^2+1} = \tau G_{1\parallel} \ . && (2.18)
\end{aligned}$$

Similar to the real space components, each diffraction spot has two indices associated to it from the square reciprocal lattice.

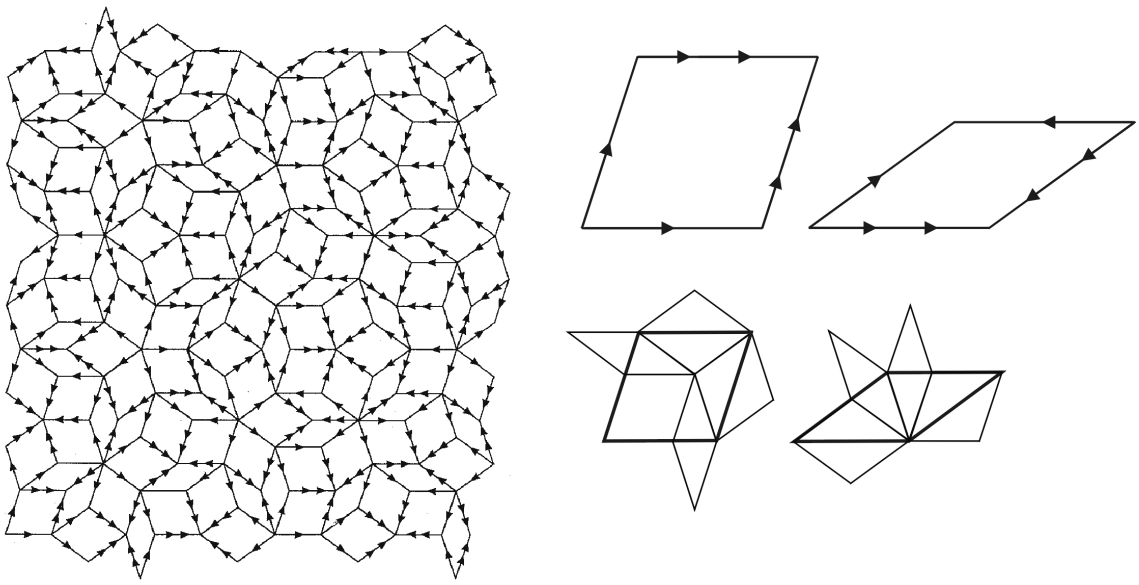

Figure 2.3: A section of the rhombic Penrose tiling obtained from the two tiles, whose edges are labeled by arrows, by following the edge matching rule (from [24]). The tenfold symmetry can be realized by a rotation of the tiling by $\pi/5$ and translation. The inflation mechanism is illustrated in the lower right part of the figure.

Hence, the cut method for construction of a Fibonacci sequence in real space corresponds to the projection method in reciprocal space. With the relations 2.5 it can be shown that the projection method in real space requires the cut method in reciprocal space to explain the features of a Fibonacci sequence [24].

2.3 The two-dimensional Penrose Tiling

The most prominent example of a 2-dimensional quasiperiodic structure is the Penrose tiling, found by Penrose in 1974 [30]. The Penrose tiling is an example of a space-filling tiling with tenfold symmetry. It consists of two different kinds of tiles, a 'skinny' (with an acute angle $\alpha_s = \pi/5 = 36°$) and a 'fat' (with an acute angle $\alpha_f = 2\pi/5 = 72°$) rhomb with equal edge length a_r and areas $A_s = a_r^2 \sin(\pi/5)$ and $A_f = a_r^2 \sin(2\pi/5)$, respectively. The areas of the two tiles as well as their frequencies are both in the ratio 1 to τ.

The perfect Penrose tiling is obtained from these tiles by following strict matching rules. These can be visualized by assigning each edge with a particular type of arrow as indicated in figure 2.3. The rule then states that neighboring tiles are only allowed if their joining edges match [24].

Like the 1-dimensional Fibonacci sequence, the Penrose tiling is also self-similar. Therefore, by inflation or deflation a Penrose tiling with τ times enlarged or reduced edge length can be obtained by following the transformation rules as indicated in the lower right part of figure 2.3. Due to these rules a fat rhombus transforms into two fat and one skinny rhombi, while one skinny rhombus is divided into one fat and one skinny rhombus.

In the approach from higher dimensional space, the Penrose tiling can be obtained as an irrational cut of a 4-dimensional hypercrystal with the 2-dimensional physical space. The 4-dimensional lattice is spanned by the basis vectors [31]

$$\mathbf{a}_j = \frac{2a}{5} \begin{pmatrix} \cos\frac{2\pi j}{5} - 1 \\ \sin\frac{2\pi j}{5} \\ \cos\frac{4\pi j}{5} - 1 \\ \sin\frac{4\pi j}{5} \end{pmatrix} \tag{2.19}$$

with $j = 1, ..., 4$ and $a = \frac{2\pi}{a^*}$ with a^* the length of the reciprocal basis vectors in physical space. The hyperrhombohedral unit cells in 4D are decorated by four pentagonal shaped atomic surfaces. These are located at positions $\frac{i}{5}(1,1,1,1)$ with $i = 1, ..., 4$ along the volume diagonal. The pentagons' faces are oriented parallel to perpendicular space and possess radii of $\lambda_{1,4} = \frac{2}{5\tau^2 a^*}$ and $\lambda_{2,3} = \frac{2}{5\tau a^*}$ [28, 32]. The pentagons 1 and 3 have the same orientation in the perpendicular space plane, while 2 and 4 are related to them by inversion symmetry.

From equation 2.19 it can be deduced that the hyperrhombohedral diagonal is directed along [1010]. Since the section of the pentagonal atomic surfaces with the [1000]-axis yields the tiling's vertices along [1000] it can be inferred that the length a_r of a Penrose rhomb in physical space is

$$a_r = \frac{2\tau^3 a}{5} \tag{2.20}$$

With the orthogonality condition $\mathbf{a}_i \cdot \mathbf{a}_j^* = 2\pi\delta_{ij}$ the basis vectors of the 4-dimensional reciprocal space are

$$\mathbf{a}_j^* = a^* \begin{pmatrix} \cos\frac{2\pi j}{5} \\ \sin\frac{2\pi j}{5} \\ \cos\frac{4\pi j}{5} \\ \sin\frac{4\pi j}{5} \end{pmatrix}, \text{with } j = 1, ...4 \ . \tag{2.21}$$

The 2-dimensional diffraction pattern corresponds to the projection of the 4D reciprocal lattice onto physical space. Hence, its basis vectors are

$$\mathbf{d}_j^* = a^* \begin{pmatrix} \cos\frac{2\pi j}{5} \\ \sin\frac{2\pi j}{5} \end{pmatrix}, \text{with } j = 1, ...4 \ . \tag{2.22}$$

2.4 The Structure Factor in Quasiperiodic Systems

The structure factor in periodic lattices is defined as the Fourier transform of the atomic density distribution function $\rho(\vec{r})$ within the unit cell

$$S(\vec{k}) = \int\limits_{unit\ cell} \rho(\vec{r}) e^{i\vec{k}\vec{r}} d\vec{r} = \sum_{l=1}^{n} \Theta_l(\vec{k}) f_l(\vec{k}) e^{i\vec{k}\vec{r}} \tag{2.23}$$

where Θ describes the Debye-Waller term, and $f_l(\vec{k})$ is the atomic form factor of the lth atom in the unit cell.

The structure factor of a quasicrystal's reciprocal lattice is somewhat more complex. Having realized that the intensity of a particular diffraction spot is dependent on its perpendicular space component, the structure factor can be divided into contributions from the conventional atomic scattering factors in parallel space $f_l(\vec{k_\parallel})$ and from a geometrical form factor $g_l(\vec{k_\perp})$ in perpendicular space:

$$S(\vec{k}) = \sum_{l=1}^{n} \Theta_l(\vec{k_\parallel}, \vec{k_\perp}) f_l(\vec{k_\parallel}) g_l(\vec{k_\perp}) e^{i\vec{k}\vec{r}} \ . \tag{2.24}$$

Compared to a periodic crystal, the non-unity geometrical form factor resulting from the Fourier transform of the atomic surfaces in perpendicular space leads to an intensity modulation of Bragg peaks not known in conventional crystallography.

2.5 Phasons

The additional dimensions of perpendicular space also have an impact on the elastic properties of quasicrystals. While excitations in parallel space correspond to the well-known phonons, an additional degree of freedom arises from excitations in perpendicular space, which are called phasons.

An illustration of this degree of freedom in the example of the Fibonacci sequence is shown in figure 2.4. A displacement of the 2-dimensional lattice and the atomic surfaces by $\vec{u}$ can be separated into a displacement along parallel and perpendicular space, i.e.,

$$\vec{u} = \vec{u}_\parallel + \vec{u}_\perp \ . \tag{2.25}$$

While periodic crystals also possess a translational degree of freedom in parallel space $\vec{u}_\parallel$, $\vec{u}_\perp$ represents an additional degree of freedom in perpendicular space of quasicrystals. A displacement $\vec{u}_\parallel$ results only in the translation of the Fibonacci sequence as indicated in figure 2.4 (c). The related elastic excitations are the phonons in conventional crystallography. In contrast, a translation $\vec{u}_\perp$ along perpendicular space introduces a local rearrangement of atoms, such as

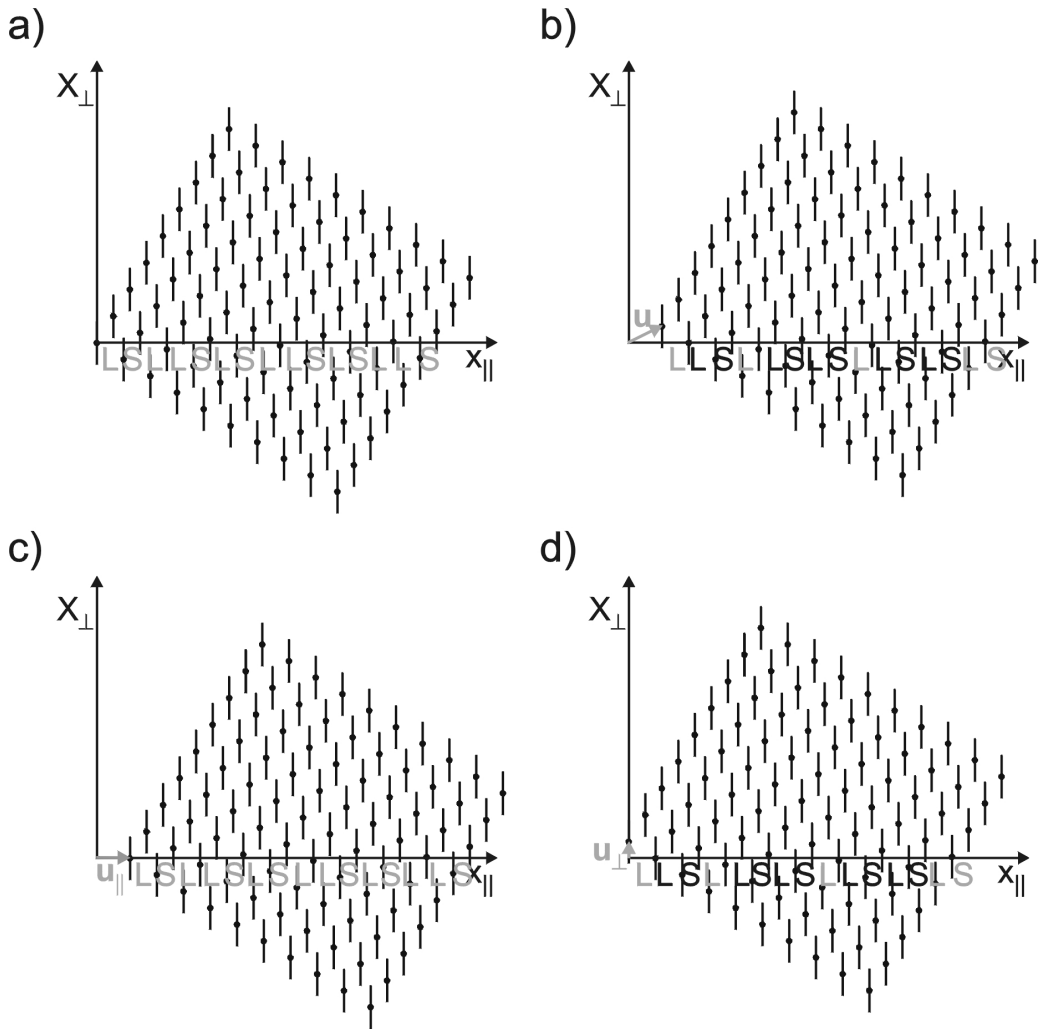

Figure 2.4: Illustration of phason flips. (a) Fibonacci sequence generated from a 2-dimensional periodic lattice. Resulting structure from a displacement (b) $\vec{u}$, (c) $\vec{u}_{\parallel}$, and (d) $\vec{u}_{\perp}$

$LS \leftrightarrow SL$, in physical space as indicated by the black letters in figure 2.4 (d). These atomic jumps are also called phason flips. The corresponding phason strain leading to the atom jumps is $\frac{d\vec{u}_{\perp}}{d\vec{r}_{\parallel}}$ in analogy to the elastic strain in conventional crystals $\frac{d\vec{u}_{\parallel}}{d\vec{r}_{\parallel}}$. Phason flips are regarded as a key mechanism for structural phase transitions [33] and will therefore come into play in chapter 4.

As already indicated in equation 2.24 the intensity of the diffraction spots is not only reduced by the phonon related Debye-Waller factor, but also by a phasonic Debye-Waller term [34]. Recently, single atom jumps were observed experimentally by transmission electron microscopy and their vibrational properties were studied [35]. Phason fluctuations with a non-zero average

displacement can lead to peak broadening and a shift of the quasicrystalline diffraction spots [36]. Collective phason flips leading to a deformation of the tiling underlying the quasicrystalline structure have been observed by Edagawa et al. [37].

2.6 Approximants

It has been illustrated in the previous section that a non-zero average atomic displacement resulting from a phason strain leads to a change of atom positions. A linear phason strain yields a shearing of the 2-dimensional lattice along perpendicular space as illustrated in figure 2.5. For small shear displacements of the atoms their new positions can be approximated by a tilt of the periodic lattice with respect to physical space. If thereby an angle α with $\tan\alpha$ irrational is achieved, a periodic atomic arrangement results. If the corresponding angle approximates the original one of $\arctan 1/\tau$ by $\arctan 1/1$, $\arctan 1/2$, $\arctan 2/3$, $\arctan 3/5$ or $\arctan 5/8$ etc. which is the ratio of successive Fibonacci numbers, the atomic structure is called approximant. The repetition length, i.e., the size of the unit cell depends on the angle. For example, an angle of $\arctan 1/2$ leads to the structure in figure 2.5 with a repetition length of LSL. This approximant is called 2/1 approximant. The higher the order of the approximant the more similar its atomic structure is to that of the quasicrystal. Approximants are useful for modeling the atomic structure of quasicrystals in order to determine physical properties, such as the electronic structure [38-41].

2.7 Decagonal Quasicrystals

One class of stable quasicrystals discovered so far are the decagonal quasicrystals. They possess quasicrystalline planes, which are periodically stacked along the tenfold rotational axis. While the quasiperiodic planes obey a fivefold symmetry, the overall tenfold rotational symmetry arises from the stacking of planes where fivefold objects in adjacent planes are related by inversion symmetry. The quasicrystalline planes can be characterized by a Penrose tiling whose vertices are decorated with atomic clusters.

From the sketch in figure 2.6 three high symmetry surface orientations can be inferred in decagonal quasicrystals. First the tenfold quasicrystalline planes, and second, two kinds of twofold planes which include the periodic axis. One set corresponds to the faces of a decagonal prism, while the other set is rotated by 18° with respect to the latter. The planes are characterized by their Miller indices, which will be introduced in section 2.7.2.

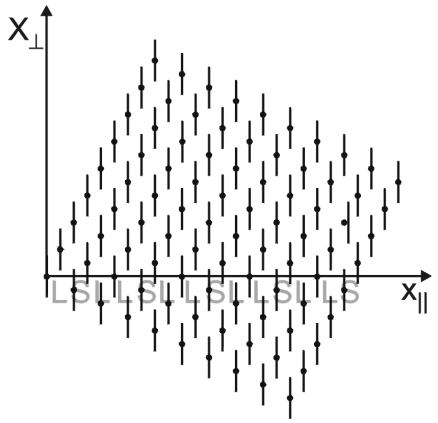

Figure 2.5: Illustration of an approximant structure with a repetition length of LSL resulting from a linear phason strain.

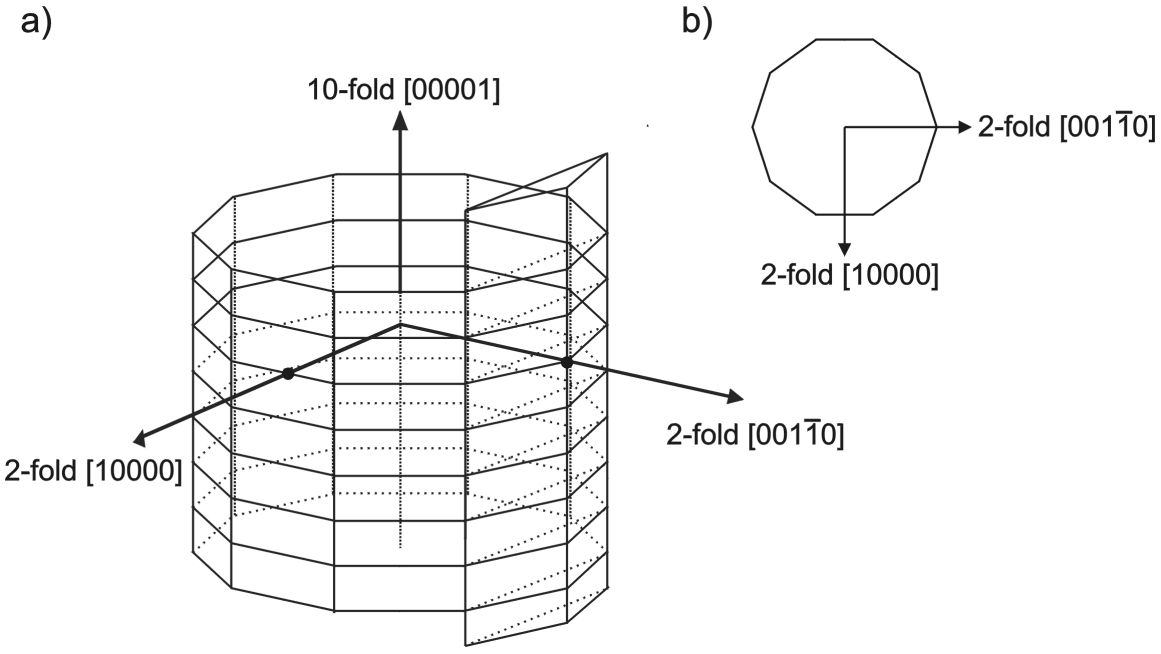

Figure 2.6: Schematic representation of a decagonal quasicrystal in (a) perspective view, (b) top view on quasicrystalline planes.

2.7.1 Atomic Structure

As already mentioned, decagonal quasicrystals can be characterized by a stacking of Penrose tilings. The derivation of a periodic sequence of Penrose tilings from higher dimensional space is similar to the approach described in section 2.3. In order to include the periodic axis a 5-dimensional hyperspace is needed for the derivation. Thus, the basis vectors are [32]

$$\mathbf{a}_j = \frac{2a}{5}\begin{pmatrix} \cos\frac{2\pi j}{5} - 1 \\ \sin\frac{2\pi j}{5} \\ 0 \\ \cos\frac{6\pi j}{5} - 1 \\ \sin\frac{6\pi j}{5} \end{pmatrix}, j = 1,..4;\ \mathbf{a}_5 = a_5\begin{pmatrix} 0 \\ 0 \\ 1 \\ 0 \\ 0 \end{pmatrix}. \tag{2.26}$$

In order to obtain the atomic positions for the type I phase of decagonal Al-Ni-Co (the different phases will be discussed in chapter 4) Yamamoto and Weber start with the hyper unit cells of a Penrose tiling of 19.79 Å edge length (the tiling on which the atomic clusters are located) and place occupation domains at interatomic distances from the ones generating the tiling's vertices. The shapes of these occupation domains are different from those of the Penrose tiling. They only have a mirror plane (see [32]). Cervellino et al. use a different approach to model the atomic structure [42]. They refine the shape of the occupation domains and introduce occupation probabilities for the atomic species.

2.7.2 Indexing of Decagonal Quasicrystals

The reciprocal basis vectors to equation 2.26 are

$$\mathbf{a}_j^* = a^*\begin{pmatrix} \cos\frac{2\pi j}{5} \\ \sin\frac{2\pi j}{5} \\ 0 \\ \cos\frac{6\pi j}{5} \\ \sin\frac{6\pi j}{5} \end{pmatrix}, j = 1,...4;\ \mathbf{a}_5^* = a_5^*\begin{pmatrix} 0 \\ 0 \\ 1 \\ 0 \\ 0 \end{pmatrix} \tag{2.27}$$

and their projection onto physical space

$$\mathbf{d}_j^* = a^*\begin{pmatrix} \cos\frac{2\pi j}{5} \\ \sin\frac{2\pi j}{5} \\ 0 \end{pmatrix}, j = 1,...4;\ \mathbf{d}_5^* = a_5^*\begin{pmatrix} 0 \\ 0 \\ 1 \end{pmatrix}. \tag{2.28}$$

Hence, a reciprocal lattice vector can be obtained by

$$\mathbf{G} = \sum_{j=1}^{5} h_j \mathbf{d}_j^* \tag{2.29}$$

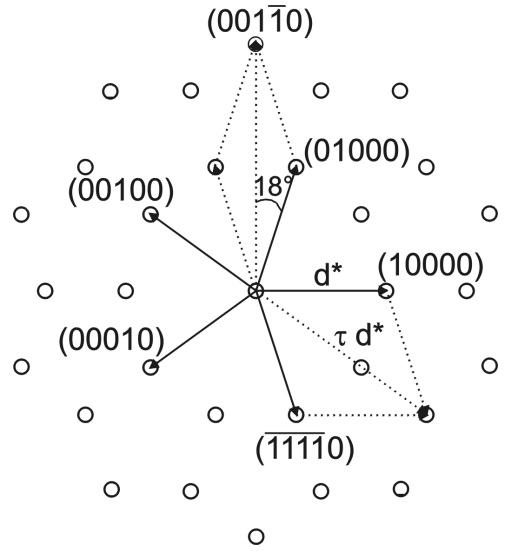

Figure 2.7: Representation of indexing reciprocal lattice vectors in the decagonal plane by the four independent vectors $\mathbf{d}_j^* = a^*(\cos\frac{2\pi}{5}, \sin\frac{2\pi}{5}, 0)$ with $j = 1, ...4$. The linear combination of independent vectors yields the τ-scaling characteristic for decagonal quasicrystals. The fifth lattice vector $\mathbf{d}_5^* = a_5^*(0, 0, 1)$ points along the periodic direction perpendicular to the plane of the paper.

with $(h_1h_2h_3h_4h_5)$ the generalized Miller indices. An illustration of the indexing scheme is shown in figure 2.7. The linear combination of independent lattice vectors thus yields the τ-scaling in the diffraction patterns, since $\tau = 2\cos\frac{\pi}{5}$.

For this thesis three inequivalent high symmetry surface orientations have been investigated. Their real space orientation has already been shown in figure 2.6. They can now be indexed by their corresponding Miller indices. Therefore, the tenfold quasicrystalline plane is referred to as (00001)-plane. The twofold planes representing the decagonal prism faces are (10000)-equivalent planes, while the other twofold planes are indexed by (001$\bar{1}$0).

For decagonal $Al_{72.3}Ni_{18.2}Co_{9.5}$ the length of the reciprocal basis vectors are $a^* = 1.03\,\text{Å}^{-1}$ and $a_5^* = 1.54\,\text{Å}^{-1}$ [42]. High resolution low energy electron diffraction patterns of the three surfaces just described are displayed in figure 2.8. The indexing of the observed diffraction peaks follows the above derived scheme and is illustrated at the right hand side of each image.

2.8 Icosahedral Quasicrystals

The quasicrystal that was first discovered, the rapidly quenched Al-Mn, belongs to the class of icosahedral quasicrystal. The most widely studied thermodynamically stable icosahedral quasicrystal is Al-Pd-Mn. In contrast to decagonal quasicrystals, icosahedral quasicrystals exhibit

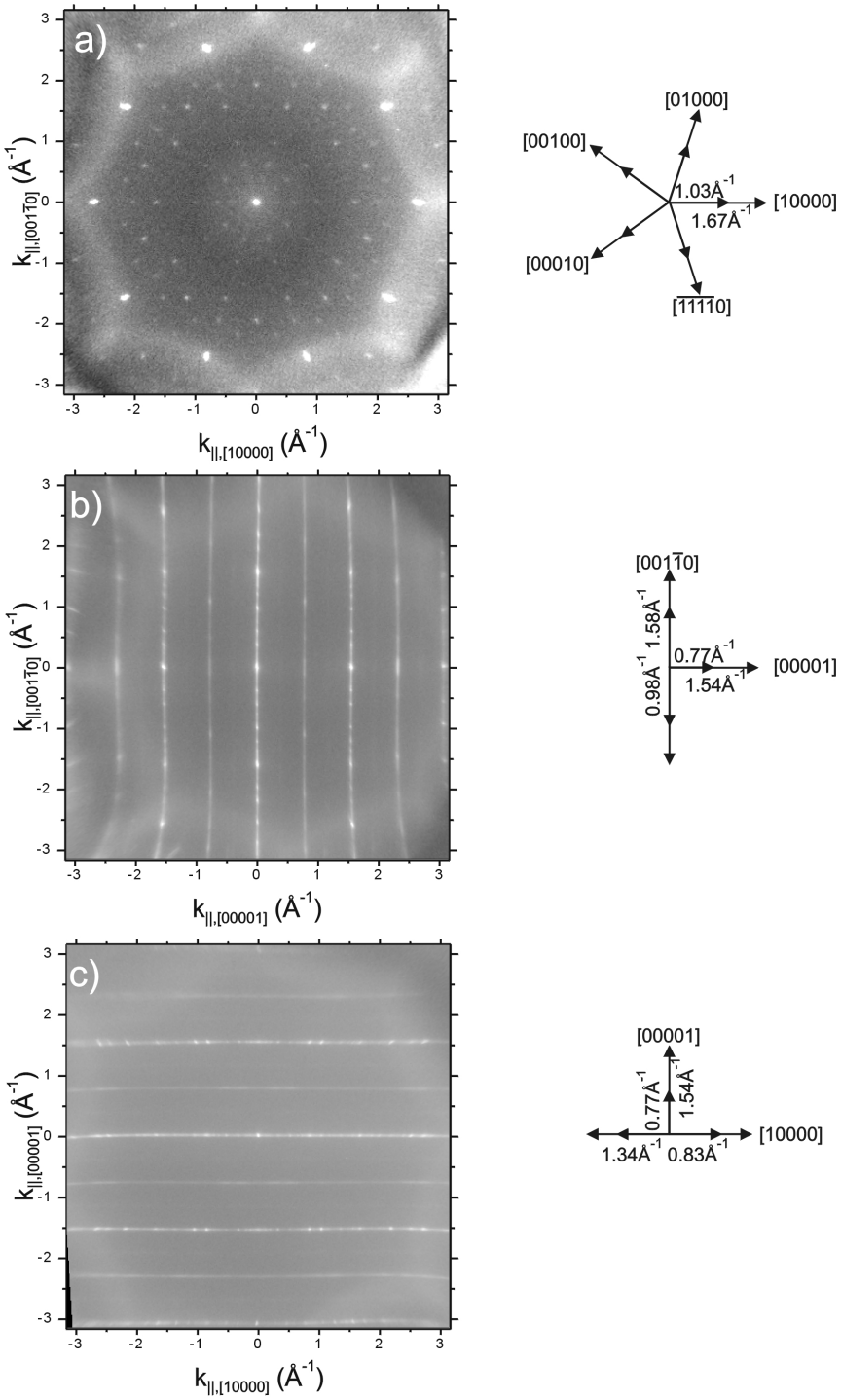

Figure 2.8: SPALEED patterns of (a) the tenfold (00001)-surface at 65 eV, (b) the twofold (10000)- surface, and (c) the twofold (00$1\bar{1}$0)-surface of decagonal $Al_{72.3}Ni_{18.2}Co_{9.5}$ with their respective indexing vectors.

an aperiodic ordering along all three real space dimensions. They possess six fivefold, ten threefold, and fifteen twofold axes. In order to derive the atomic structure a 3-dimensional cut with a 6-dimensional hyperspace is required.

2.8.1 Indexing of Icosahedral Quasicrystals

The reciprocal basis vectors in 6-dimensional space are [31]

$$\mathbf{a}_1^* = a^* \begin{pmatrix} 0 \\ 0 \\ 1 \\ 0 \\ 0 \\ 1 \end{pmatrix}, \ \mathbf{a}_j^* = a^* \begin{pmatrix} \sin\theta\cos\frac{2\pi j}{5} \\ \sin\theta\sin\frac{2\pi j}{5} \\ \cos\theta \\ -\sin\theta\cos\frac{4\pi j}{5} \\ \sin\theta\sin\frac{4\pi j}{5} \\ -\cos\theta \end{pmatrix}, j = 2,..6; \tag{2.30}$$

with θ being the angle between two adjacent twofold axes ($\tan\theta = 2$) and $\frac{2\pi}{a^*}$ the lattice constant in 6-dimensional space.

The physical space projection yields

$$\mathbf{d}_1^* = a^* \begin{pmatrix} 0 \\ 0 \\ 1 \end{pmatrix}, j = 1; \ \mathbf{d}_j^* = a^* \begin{pmatrix} \sin\theta\cos\frac{2\pi j}{5} \\ \sin\theta\sin\frac{2\pi j}{5} \\ \cos\theta \end{pmatrix}, j = 2,..6 \ . \tag{2.31}$$

Figure 2.9 illustrates the basis vectors. The basis vectors $\mathbf{d}_1^*$, ...$\mathbf{d}_6^*$ are directed from the midpoint of the icosahedron to the corners. A reciprocal lattice vector can then be characterized by six Miller indices ($h_1h_2h_3h_4h_5h_6$) via

$$\mathbf{G} = \sum_{j=1}^{6} h_j \mathbf{d}_j^* \ . \tag{2.32}$$

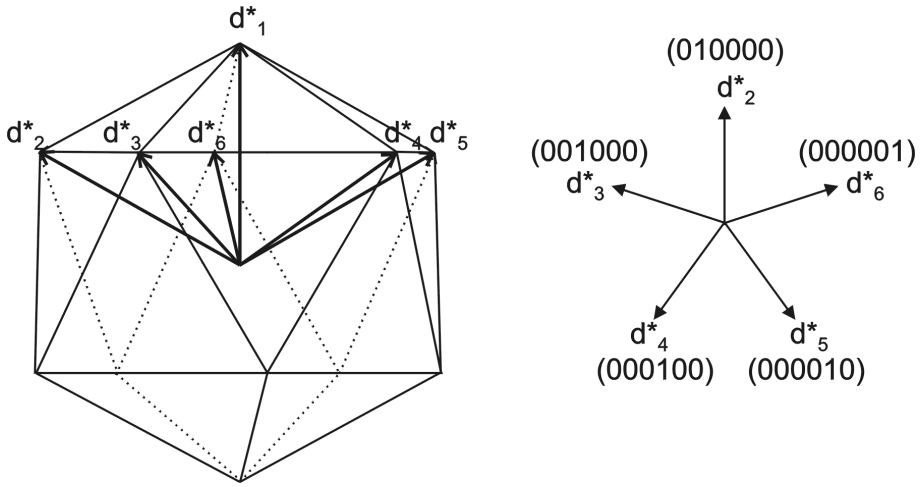

Figure 2.9: Indexing scheme for icosahedral quasicrystals: (a) side view of the reciprocal basis, (b) projection of basis vectors into the fivefold plane.